Mon. Not. R. Astron. Soc. **000**, 1–11 (2005) Printed 12 May 2005 (MN LATEX style file v2.2)

The imprints of local superclusters on the Sunyaev-Zel'dovich signals and their detectability with Planck

K. Dolag[1]⋆, F.K. Hansen[2]†, M. Roncarelli[3]‡, L. Moscardini[3]§
[1] *Max-Planck-Institut für Astrophysik, Karl-Schwarzschild-Straße 1, 85740 Garching bei München, Germany*
[2] *Institute of Theoretical Astrophysics, University of Oslo, P.O. Box 1029 Blinders, N-0315 Oslo, Norway*
[3] *Dipartimento di Astronomia, Università di Bologna, via Ranzani 1, I-40127 Bologna, Italy*

Accepted ???. Received ???; in original form May 2005

ABSTRACT
We use high-resolution hydrodynamical simulations of large-scale structure formation to study the imprints of the local superclusters onto the full-sky Sunyaev-Zel'dovich (SZ) signals. Following Mathis et al. (2002), the initial conditions have been statistically constrained to reproduce the density field within a sphere of 110 Mpc around the Milky Way, as observed in the IRAS 1.2-Jy all-sky redshift survey. As a result, the positions and masses of prominent galaxy clusters and superclusters in our simulations coincide closely with their real counterparts in the local universe. We present the results of two different runs, one with adiabatic gas physics only, and one also including cooling, star formation and feedback. By analysing the full-sky maps for the thermal and kinetic SZ signals extracted from these simulations, we find that for multipoles with $\ell < 100$ the power spectrum is dominated by the prominent local superclusters, and its amplitude at these scales is a factor of two higher than that obtained from unconstrained simulations; at lower multipoles ($\ell < 20$) this factor can even reach one order of magnitude. We check the influence of the SZ effect from local superclusters on the cosmic microwave background (CMB) power spectrum at small multipoles and find it negligible and with no signs of quadrupole-octopole alignment. However, performing simulations of the CMB radiation including the experimental noise at the frequencies which will be observed by the Planck satellite, we find results suggesting that an estimate of the SZ power spectrum at large scales can be extracted.

Key words: cosmology: cosmic microwave background, observations – methods: numerical – galaxies: clusters: general

1 INTRODUCTION

It is well known that high-accuracy measurements of the anisotropies of the cosmic microwave background (CMB) are extremely important for cosmology. By analysing their angular power spectrum, $C(\ell)$, it is in fact possible to obtain tight constraints on the mechanisms from which the primordial fluctuations originate and on the main cosmological parameters (or combinations of them) like the matter density, the baryonic density and the cosmological constant contribution. For this reason, the astronomical community has been doing a big effort over the last years in order to improve the quality of the CMB data, both in terms of accuracy and resolution.

The best available CMB measurements up to now were provided by the *Wilkinson Microwave Anisotropy Probe* satellite (WMAP; Bennett et al. 2003). The data obtained in its first year of activity gave strong support to the so-called concordance model, i.e. a spatially flat universe dominated by dark energy and cold dark matter, with nearly scale-invariant primordial fluctuations, almost gaussianly distributed. The WMAP result is confirming the general picture emerging by the analysis of other different datasets, like high-redshift supernovae Ia, weak lensing, galaxy survey, Lyman-α forest and galaxy clusters (see discussion in Spergel et al. 2003, and references therein).

The statistical analysis and the theoretical interpretation of CMB data of so high quality necessarily require a good understanding of all possible sources of contamination as well as the techniques to separate them from the CMB signal. The Sunyaev-Zel'dovich (SZ) effect (Sunyaev & Zeldovich 1972), i.e. the Compton scatter of the cold CMB photons by the hot electrons mainly located in the intracluster plasma, certainly represents one of the most important secondary anisotropies, i.e. temperature fluctuations generated along the light trajectory from the last scattering surface to the observer. Different studies have been devoted to the estimate of the SZ angular power spectrum which originates from

⋆ E-mail: kdolag@mpa-garching.mpg.de
† E-mail: f.k.hansen@astro.uio.no
‡ E-mail: mauro.roncarelli@studio.unibo.it
§ E-mail: lauro.moscardini@unibo.it

the whole galaxy cluster population (see, e.g., Cooray et al. 2004, and references therein). The results show that the SZ signal starts to dominate the cosmological one only on very small angular scales ($\ell > 2000$), while at the scales covered by WMAP is approximately 3 orders of magnitude smaller.

Even if its amplitude appears relatively small, the SZ signal could be nevertheless significant at the sky positions corresponding to nearby galaxy clusters. This has motivated the research of SZ imprints in the first-year WMAP temperature maps. This approach, mainly based on the cross-correlation of the CMB maps with the observed distribution of clusters and superclusters, as extracted in both optical and X-ray surveys, led to different claims for a positive detection at small angular scales (Myers et al. 2004; Hernández-Monteagudo & Rubiño-Martín 2004; Fosalba & Gaztañaga 2004; Afshordi et al. 2004), but only upper limits for the detection of the SZ signal exist at larger scales at present (Diego et al. 2003; Hernandez-Monteagudo et al. 2004; Hirata et al. 2004; Huffenberger et al. 2004; Hansen et al. 2005). In this sense the situation will largely improve in the near future thanks to the capabilities of the *Planck* satellite, whose launch is planned for 2007. In fact the range of frequencies covered by its receivers will be very large, and the noise level is expected to be very low. This will allow to extract the SZ signal for at least 10,000 objects out to redshfit $z \approx 1$ (see, e.g. Bartelmann 2001).

The CMB data from the WMAP satellite exhibit several anomalies at the lowest multipoles, among them the abnormally low value of the quadrupole amplitude (see, however, Efstathiou 2004) and the fact that the direction of the quadrupole and octopole are unusually well aligned (see, e.g., Gaztañaga et al. 2003; de Oliveira-Costa et al. 2004). There have been some speculation about the possibility that the SZ signal from structures in the local universe (the so-called local supercluster) could be the cause of the low quadrupole (Abramo & Sodre 2003). Further, the quadrupole and octopole directions happen to be pointing toward the Virgo cluster (de Oliveira-Costa et al. 2004), which opens the possibility of contamination from the local universe.

The goal of this paper is to investigate the importance of the thermal and kinetic SZ effects produced by the local superclusters by comparing it with respect to the cosmological signal and to the contribution of more distant clusters. At this aim we will use the results of high-resolution hydrodynamical simulations realized starting from initial conditions (Mathis et al. 2002) which are constrained to reproduce the density field recovered by the IRAS 1.2-Jy all-sky redshift survey. Using full-sky maps extracted from these numerical simulations, we will discuss the statistical properties of low multipoles in terms of amplitude and alignment. Moreover, taking advantage of the different set of physical processes treated in the simulations we can assess the uncertainties related to the modelization. Finally we will perform simulations to discuss if the local SZ signal can be detected exploiting the capabilities of the Planck satellite.

The plan of the paper is as follows. In Section 2 we describe the general characteristics of the constrained hydrodynamical simulations of the local universe used in the following analysis. Section 3 presents our method to produce full-sky maps of the thermal and kinetic SZ effects. Section 4 is devoted to the results of our analysis. In particular we show the statistical properties of the maps in terms of angular power spectra and alignment of lower multipoles and we discuss the possibility of detecting the local SZ signal with future experiments, like the upcoming Planck satellite. Finally we summarize our findings and draw the main conclusions in the final Section 5.

2 THE CONSTRAINED HYDRODYNAMICAL SIMULATIONS

The results presented in this paper have been obtained by using the final output of two different cosmological hydrodynamical simulations of the local universe obtained starting from the same initial conditions but following a different set of physical processes. In more detail we used initial conditions similar to those adopted by Mathis et al. (2002) in their study (based on a pure N-body simulation) of structure formation in the local universe. The galaxy distribution in the IRAS 1.2-Jy galaxy survey is first gaussianly smoothed on a scale of 7 Mpc and then linearly evolved back in time up to $z = 50$ following the method proposed by Kolatt et al. (1996). The resulting field is then used as a Gaussian constraint (Hoffman & Ribak 1991) for an otherwise random realization of a flat ΛCDM model, for which we assume a present matter density parameter $\Omega_{0m} = 0.3$, a Hubble constant $H_0 = 70$ km/s/Mpc and a r.m.s. density fluctuation $\sigma_8 = 0.9$. The volume that is constrained by the observational data covers a sphere of radius ~ 110 Mpc, centred on the Milky Way. This region is sampled with high-resolution dark matter particles and is embedded in a periodic box of ~ 343 Mpc on a side. The region outside the constrained volume is filled with low-resolution dark matter particles, allowing a good coverage of long-range gravitational tidal forces.

The statistical analysis made by Mathis et al. (2002) demonstrated that the evolved state of these initial conditions provides a good match to the large-scale structure observed in the local universe. Using semi-analytic models of galaxy formation built on top of merging history trees extracted from the dark matter distribution in the simulation, they showed that the density and velocity maps obtained from synthetic mock galaxy catalogues have characteristics very similar to their observational counterparts. Moreover many of the most prominent nearby galaxy clusters like Virgo, Coma, Pisces-Perseus and Hydra-Centaurus, can be identified directly with haloes in the simulation, with a good agreement for sky positions and virial masses. In fact the positions of all identified objects differ less than the smoothing radius adopted in the initial conditions (7 Mpc), with the only exception of Centaurus, which is displaced by 9.6 Mpc. The agreement for the masses is within a factor of 2 which can be considered acceptable if one considers the uncertainties in the inferred observational masses, mainly when velocity dispersion is used.

Unlike in the original simulation made by Mathis et al. (2002), where only the dark matter component is evolved, here we want to follow also the gas distribution. For this reason we extended the initial conditions by splitting the original high-resolution dark matter particles into gas and dark matter particles having masses of $0.69 \times 10^9\ M_\odot$ and $4.4 \times 10^9\ M_\odot$, respectively. Consequently the most massive clusters in our simulations will be resolved by almost one million particles.

Our runs have been carried out with GADGET-2 (Springel 2005), a new version of the parallel Tree-SPH simulation code GADGET (Springel et al. 2001). The code uses an entropy-conserving formulation of SPH (Springel & Hernquist 2002), and allows a treatment of radiative cooling, heating by a UV background, and star formation and feedback processes. The latter is based on a sub-resolution model for the multiphase structure of the interstellar medium (Springel & Hernquist 2003). The code can also follow the pattern of metal production from the past history of cosmic star formation (Tornatore et al. 2004). This is done by computing the contributions from both Type-II and Type-Ia supernovae and energy feedback and metals are released gradually in time, accordingly to the appropriate lifetimes of the different stellar populations. This treatment also includes in a self-consistent way the dependence of the gas cooling on the local metallicity.

As said, the results presented in this work are based on two different simulations starting from the same initial conditions. The first one, hereafter called *gas*, includes only non-radiative (i.e. adiabatic) hydrodynamics and has been originally analyzed by Dolag et al. (2005) to study the propagation of cosmic rays in the local universe. Hansen et al. (2005) used the gas properties extracted from this simulation to infer a prediction of the SZ effect from diffuse hot gas in the local universe. The second run, hereafter called *csf*, exploits all the capabilities of the present version of the GADGET code, including cooling, star formation, feedback and metallicity; its outputs will be also used to study the detectability of the diffuse, warm intergalactic medium with future X-ray experiments (Yoshikawa et al. in preparation).

The gravitational force resolution (i.e. the comoving softening length) of both simulations has been fixed to be 10 kpc, which is comparable to the interparticle separation reached by the SPH particles in the dense centres of our simulated galaxy clusters.

In Table 1 we report the main characteristics of the most prominent clusters in our simulations. In particular, we computed the (mass-weighted) temperature within one tenth of the virial radius, and the central Compton-y parameter. In agreement with previous results in the literature (see, e.g., Tornatore et al. 2003), we find that the temperatures for a given object in the *csf* simulation are always larger than in the *gas* simulation by a factor of approximately 15-20 per cent. Including radiative cooling causes in fact a lack of pressure support, with a subsequent heating of the infalling gas by adiabatic compression. The opposite trend is present for the central Compton-y parameter, which can be larger by a factor up to 2 in the *gas* simulation than in the *csf* one (see also White et al. 2002; da Silva et al. 2004; Motl et al. 2005). For completeness, we also list the available observational estimates, which are in rough agreement. Notice that only for Coma we averaged in the simulation the value for Compton-y within an area of 450 kpc to be compatible with the beam size of the observational data (Battistelli et al. 2003). Finally we would like to remark that the observed temperatures are not directly comparable with the simulation results, because they are extracted from spectroscopic X-ray data: as shown by Mazzotta et al. (2004) (see also Rasia et al. 2005; Vikhlinin 2005), there could be a significant bias produced by the complexity of the thermal structure.

3 FULL SKY MAP MAKING

Hot electrons, which are present in the intracluster medium, scatter by inverse Compton the cold photons of the cosmic microwave background (CMB) radiation and re-distribute them towards higher frequencies. The result is the so-called SZ effect (Sunyaev & Zeldovich 1972) which originates a temperature decrement below 217 GHz, and an increment above.

Given a direction $\vec{\theta}$, the change of the CMB temperature $T_{\rm CMB}$ produced by the thermal SZ effect is given by

$$\frac{\Delta T_{\rm CMB}}{T_{\rm CMB}} = y(\vec{\theta})g(x)\ , \tag{1}$$

where $g(x) = x \cdot \coth(x/2) - 4$ and $x \equiv h\nu/kT_{\rm CMB}$.

The Compton-y parameter is related to the three-dimensional thermal electron density, n_e, and to the electron temperature, T, by

$$y(\vec{\theta}) = \frac{k\sigma_T}{m_e c^2}\int {\rm d}l\ n_e(\vec{\theta},l)\ T(\vec{\theta},l)\ , \tag{2}$$

σ_T being the Thomson scattering cross section.

The kinetic SZ effect is produced by the motion of the intracluster gas with respect to the CMB. The corresponding change of the CMB temperature can be written as

$$\frac{\Delta T_{\rm CMB}}{T_{\rm CMB}} = -w(\vec{\theta})\ , \tag{3}$$

with

$$w(\vec{\theta}) = \frac{\sigma_T}{c}\int {\rm d}l\ n_e(\vec{\theta},l)\ v_r(\vec{\theta},l)\ , \tag{4}$$

where v_r is the radial component of the cluster velocity.

The line of sight integrals which are present in the definitions of y (eq. 2) and w (eq. 4) can be computed in the simulations by exploiting the SPH kernel. Here we employ the spline kernel defined as (Monaghan & Lattanzio 1985)

$$W(r/h) = \frac{\pi}{h^3}\left\{\begin{array}{ll} 1-\frac{3}{2}(r/h)^2+\frac{3}{4}(r/h)^3 & 0 \leqslant (r/h) \leqslant 1 \\ \frac{1}{4}(2-r/h)^3 & 1 \leqslant (r/h) \leqslant 2 \\ 0 & 2 \leqslant (r/h) \end{array}\right. , \tag{5}$$

where h is the so-called SPH smoothing length and r represents the impact parameter. In this way eq.(2) becomes

$$y_{\rm int} = \int \sum_j \frac{m_j}{\rho_j} y_j W(d_j(r)/h_j){\rm d}r\ , \tag{6}$$

where m_j and ρ_j are the mass and density of the j-th gas particle, y_j is the corresponding Compton y-parameter and $d_j(r)$ is the projected distance with respect to the position r along the line of sight. A similar relation can be written for $w_{\rm int}$.

In principle the sum has to be done over all particles, but in the case of a compact kernel where $W(r/h)$ gets zero at large r/h (as the one we use) it can be restricted to those particles having a distance from the line of sight smaller than twice their smoothing length.

In practice, however, one would like to obtain the value averaged over all lines of sight crossing the pixel, instead of the value along the line of sight crossing the centre of the pixel only. This can become a problem when the projected size of the structure producing the signal gets smaller than the pixel size. Therefore one usually applies the so called *gather approximation*, where, given a pixel, all particles - whose projections either overlap or completely fall inside the pixel - are taken into account. In this case the value of the Compton-y parameter can be written as the sum of the contributions of all relevant particles as:

$$y_{\rm pix} = \sum_j \frac{m_j}{\rho_j} y_j N_j \frac{A_{\rm pix}}{A_j} W_{\rm int}(\tilde{d}_j/h_j)\ , \tag{7}$$

where $\tilde{d}_j$ is the projected distance between the particle and the pixel centre and $W_{\rm int}$ is the integrated kernel. The area A_j associated to each gas particle can be approximated as the square of the cubic root of the corresponding volume, i.e. $A_j = (m_j/\rho_j)^{2/3}$. The normalization factor N_j is given by

$$\sum_{\rm pix} N_j A_{\rm pix} W_{\rm int}(\tilde{d}_j/h_j) = A_j \tag{8}$$

to ensure the conservation of the quantity y when distributed over more than one pixel.

The method needs two further corrections. First, for pixels

Cluster	$T_{\rm obs}$[kev]	$T_{\rm gas}$[kev]	$T_{\rm csf}$[kev]	$y_{\rm obs}[10^{-5}]$	$y_{\rm gas}[10^{-5}]$	$y_{\rm csf}[10^{-5}]$
Coma	$8.21^{+0.16}_{-0.16}$	6.1	7.1	$9.6^{+1.1}_{-1.1}$	9.2	6.4
Virgo	$2.55^{+0.07}_{-0.06}$	3.5	4.0		4.8	3.1
Centaurus	$3.54^{+0.08}_{-0.08}$	3.8	4.4		6.7	4.2
Hydra	$3.10^{+0.11}_{-0.11}$	3.2	4.3		9.3	4.2
Perseus	$6.33^{+0.21}_{-0.18}$	5.8	6.0		9.5	6.8
A3627	$5.62^{+0.12}_{-0.11}$	3.7	4.3		6.6	4.2

Table 1. Comparison of the properties of the 6 most prominent clusters, listed in Column 1. The observed cluster temperatures $T_{\rm obs}$ (Column 2) are taken from Mohr et al. (1999), with the exception of the data for Virgo (Sanderson et al. 2003) and A3627 (Ikebe et al. 2002). Columns 3 and 4 refer to the mass-weighted temperature within $0.1 \times R_{\rm vir}$, as computed in the *gas* and *csf* simulations ($T_{\rm gas}$ and $T_{\rm csf}$, respectively). In Column 5 we report the value for the Compton-y parameter, as obtained for Coma by Battistelli et al. (2003). Columns 6 and 7 refer to the values for y computed in the *gas* and *csf* simulations ($y_{\rm gas}$ and $y_{\rm csf}$, respectively). For Coma we averaged the Compton-y within an area of 450 kpc to be compatible with the beam size of the observational data (Battistelli et al. 2003).

which are only partially overlapped by the projected SPH smoothing kernel, we approximate the associated area $\hat{A}_{\rm pix}$ as

$$\hat{A}_{\rm pix} = \sqrt{A_{\rm pix}} \times (\tilde{d}_j + 0.5\sqrt{A_{\rm pix}} - h_j) \, . \qquad (9)$$

To compute the contribution to such a pixel, the weight of the integrated kernel $W_{\rm int}$ is then corrected by a factor $\hat{A}_{\rm pix}/A_{\rm pix}$. This must be taken also into account when normalizing the integrated kernel.

Second, when a particle contributes to one pixel only, we fix the integrated kernel $W_{\rm int}$ to be unity. This is important when the area associated to such particle is much smaller than the pixel area and ensures that the value corresponding to the particle is completely given to this pixel: in this case the normalization factor N_j can become significantly smaller than unity to ensure the conservation of the quantities. Finally we notice that, since the SZ effect is independent of distance, no distance factor has to be included into the previous equations.

Figure 1 exemplifies the three different situations previously discussed by showing how the gas particles can contribute to one pixel (here represented by the square). In such cases, the weight contributed by particle 1 (shown in red) is $A_1/A_{\rm pix}$, the weight for particle 2 (in green) is $W_{\rm int}(r_2/h_2)\hat{A}_2/A_2$ and the weight for particle 3 (in blue) is $W_{\rm int}(r_2/h_2)A_{\rm pix}/A_3$. Note that for particles 2 and 3 the weight needs to be normalised to unity when summed over all pixels to which the particles are contributing.

Our maps have been constructed by applying the previous technique directly to the HEALPIx representation of the full sky (Górski et al. 1998). We fix the *nside* parameter to be 1024, which results in an all-sky representation with $\approx 1.2 \times 10^7$ pixels. In order to avoid spurious effects the line of sight integral has been performed between a minimum and maximum distance ($r_{\rm min}$ and $r_{\rm max}$, respectively). In particular we fix $r_{\rm min} = 5$ Mpc to be sure that the observer is outside the SPH smoothing radius of all particles, and $r_{\rm max} = 110$ Mpc, which represents a conservative limit of our high-resolution region.

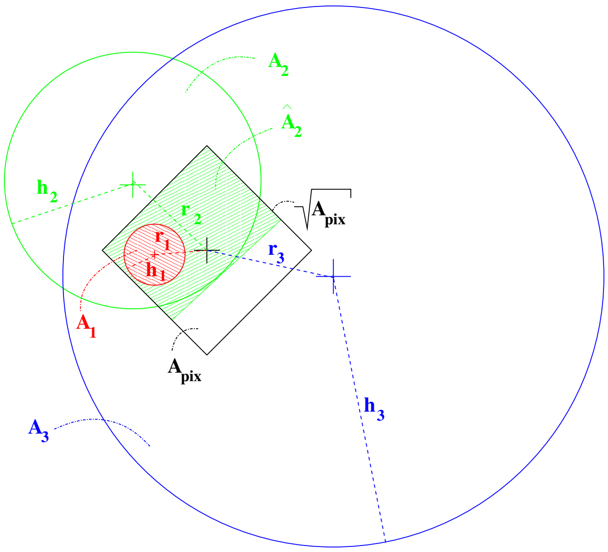

Figure 1. Sketch of three different geometrical situations for particles contributing to one pixel (represented by the black square). Particle 1 (in red), having a smoothing length h_1 and being at a distance r_1 from the pixel centre, falls completely inside the pixel, but does not overlap the centre. Particle 2 (in green) covers only partially the pixel. For particle 3 (in blue) the whole pixel lies within its projected radius.

4 RESULTS

4.1 Full-sky maps

In Fig. 2 we show the results of the application of the previous method to obtain a full-sky map of the Compton-y parameter in supergalactic coordinates. The upper panel corresponds to the signal resulting from our *gas* simulation, covering the local universe up to 110 Mpc. It is possible to recognize the most prominent features: Perseus, Virgo, Centaurus, Hydra, A3627 and Coma (very close to the northern pole of the map). Also the presence of the filamentary structure connecting the largest clusters is still evident. In the lower panel we show the same map where we add the contribution coming from more distant objects. This has been computed by exploiting the results of Schaefer et al. (2004a,b), who build SZ signal maps by using the *Hubble volume simulation* (Colberg et al. 2000; Jenkins et al. 2001) and suitably inserting the outputs of different hydrodynamic re-simulations of single clusters. Notice that the physical processes considered in these re-simulations, i.e. non-radiative hydrodynamics, are the same included in our *gas* simulation, so no biases are introduced in combining the results. With respect to the Schaefer et al. (2004) work we add only the objects having a distance from the observer larger than 110 Mpc, because the closer ones are already represented in our simulation. The resulting map appears more patchy, having a significant contribution coming from a large number of distant clusters.

The corresponding maps for the kinetic SZ signal w are shown in Fig. 3. Again the most important structures of the local universe are evident in the upper map and continue to give the dominant

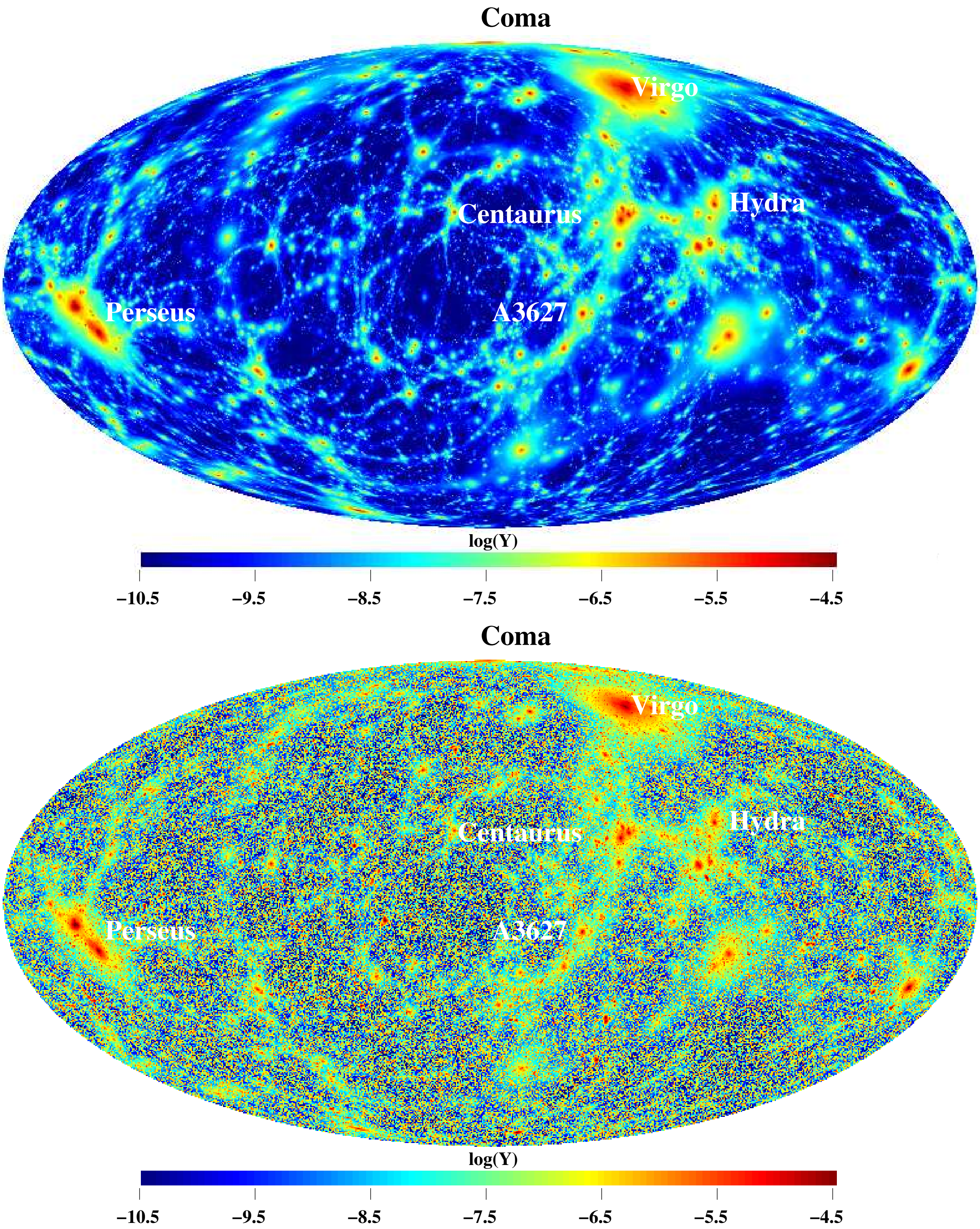

Figure 2. Full-sky map of Compton-y parameter in galactic coordinates. The upper panel shows the results from the *gas* simulation, covering the local universe up to 110 Mpc from the Milky Way, while in the lower panel we added the contribution from more distant objects, as estimated by Schaefer et al. (2004a). The position of the most prominent structures is indicated in the maps.

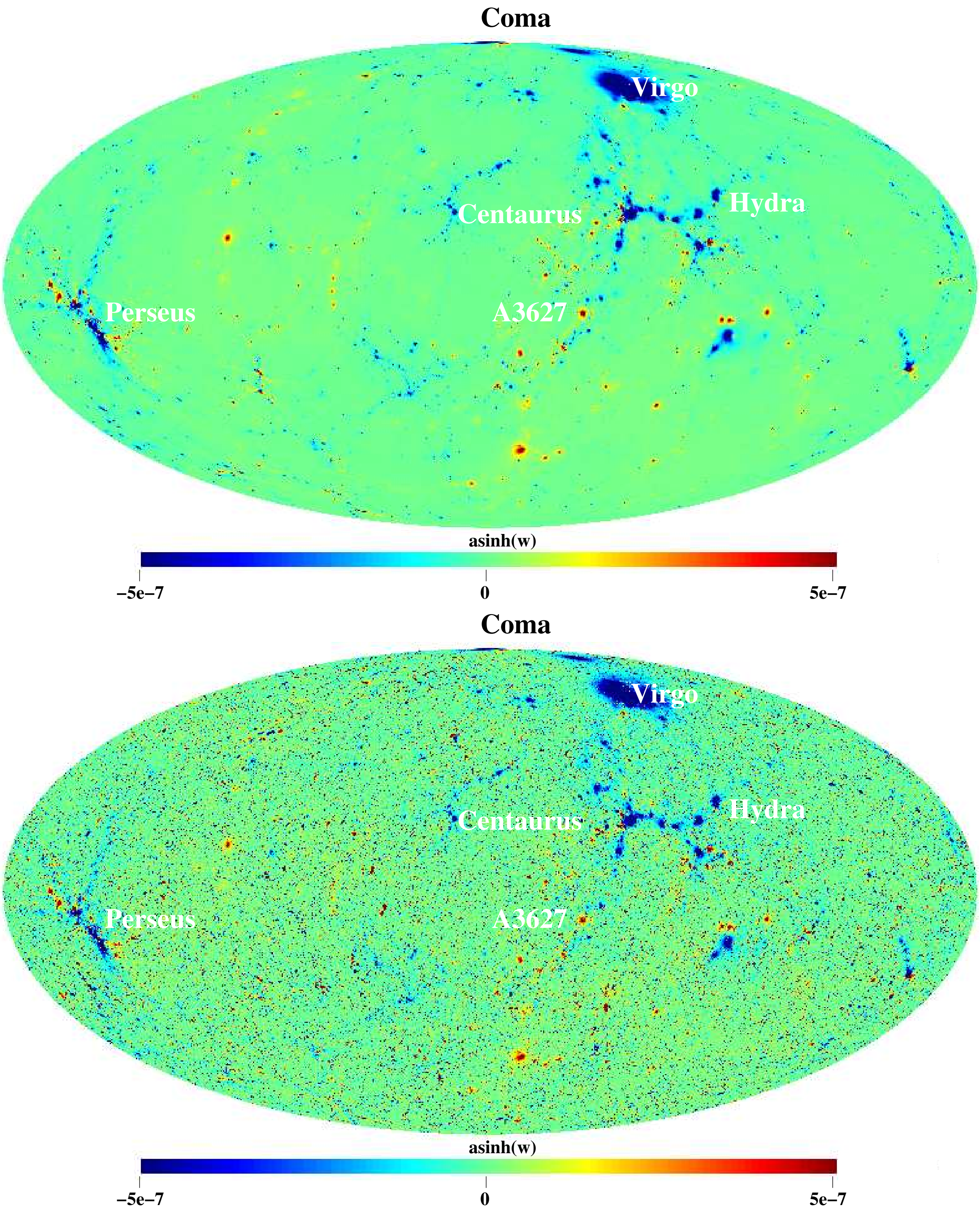

Figure 3. The same as Fig.2, but for the kinetic SZ effect, shown by using $\mathrm{asinh}(w)$ to better display positive and negative values.

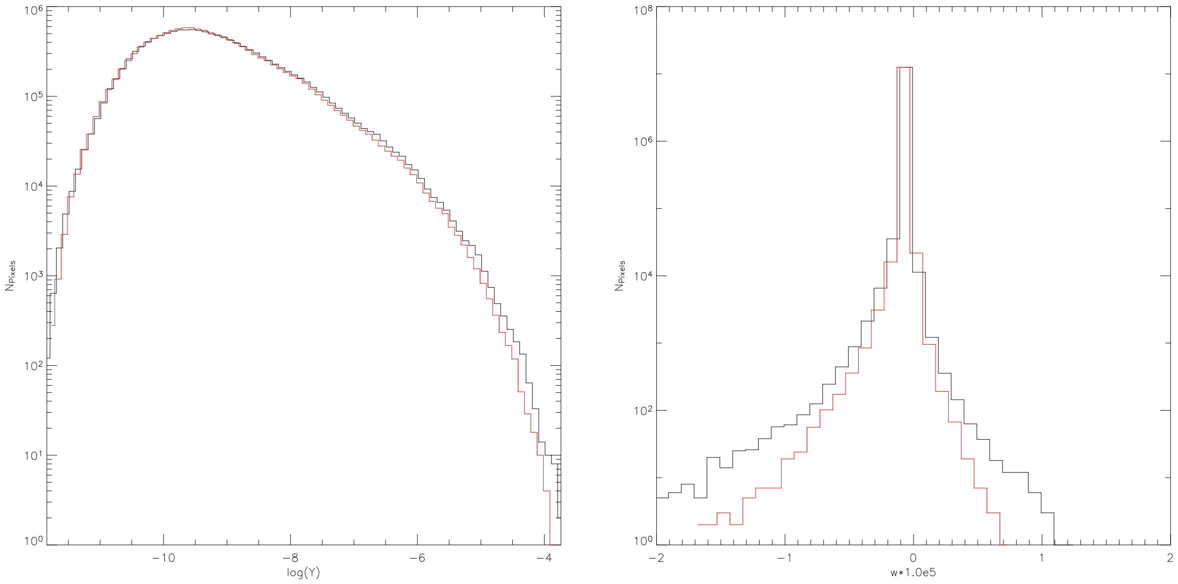

Figure 4. Comparison between the SZ signals as extracted from the *gas* and *csf* simulations (black and red lines, respectively). The number of pixels having a given value for the Compton-y parameter and the kinetic parameter w are shown in the left and right panels, respectively.

contribution in the map including distant objects, shown in lower panel.

It is worth to notice that within the simulation we measure a velocity at the observer' position of $v_x \approx -270$ km/s, $v_y \approx 420$ km/s and $v_z \approx -350$ km/s (assuming supergalactic coordinates). This leads to a absolute velocity of $v \approx 610$ km/s, which is in good agreement with the observed value (see, e.g., the WMAP analysis by Bennett et al. 2003). Again, the observer' velocity points toward a direction which differs from the observed one less than 10 degrees: this emphasizes once more that our simulations are giving a good representation of the large-scale structure in our local universe.

By analysing the maps obtained from the results of the *csf* simulation (not shown here) we find only small differences with respect to the previous results, mainly in correspondence of the high-density regions, where the *cfs* simulation tends to give smaller signals. This difference can be quantified by looking to the pixel distribution as a function of y and w. This is shown in Fig.4 where the contribution of the local universe only is considered. Concerning the thermal SZ effect (left panel), the histograms are in general very similar, with only a slightly higher frequency for higher values in the *gas* simulation. The differences are more evident in the pixel distributions for the kinetic parameter w: again high (absolute) values have higher probability in the *gas* simulation than in the *csf* one. Notice that the distribution for w is clearly non-gaussian, with a more extended tail toward negative values, produced by the cluster motion inside the local universe. Since the spectral signature of the kinetic SZ effect is the same of CMB, a perfect removal of this contribution could be difficult.

4.2 The angular power spectrum

In order to quantify the amount of signal produced by the SZ effects, we compute from our maps the angular power spectrum $C(\ell)$. In particular we estimate the spectra in the Rayleigh-Jeans region, where $\Delta T_{\rm CMB}/T_{\rm CMB} = -2y$.

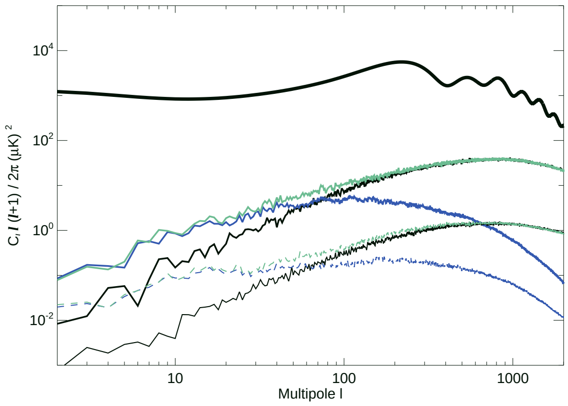

Figure 5. The power spectra for the SZ effects. Comparison between the cosmological CMB power spectrum (upper black solid lined) and the SZ signals obtained in the different simulations: *Hubble volume simulation* (black lines), local constrained *gas* simulation (blue lines); local constrained *gas* simulation combined with the *Hubble volume simulation* for larger distances (green lines). Upper and lower curves refer to the contributions from thermal and kinetic SZ effects, respectively. All spectra are taken in the Rayleigh-Jeans region where $\Delta T_{\rm CMB}/T_{\rm CMB} = -2y$.

The results are shown in Fig.5, where we compare the power spectrum of the primordial CMB radiation (here represented by the upper black line corresponding to the best fit of the WMAP data obtained by Spergel et al. 2003) to the signals extracted from the numerical simulations here considered. In particular the plot shows $C(\ell)$ for the *gas* simulation and distinguishes the contributions coming from the local universe from the one produced by more distant galaxy clusters. Both the thermal and kinetic SZ effects are considered. The results confirm that for $\ell < 2000$ the cosmological signal is dominating the SZ one, being approximately 3-4 orders of magnitude larger. Moreover the kinetic signal is always smaller by a factor of 10-20 than that produced by the thermal SZ effect.

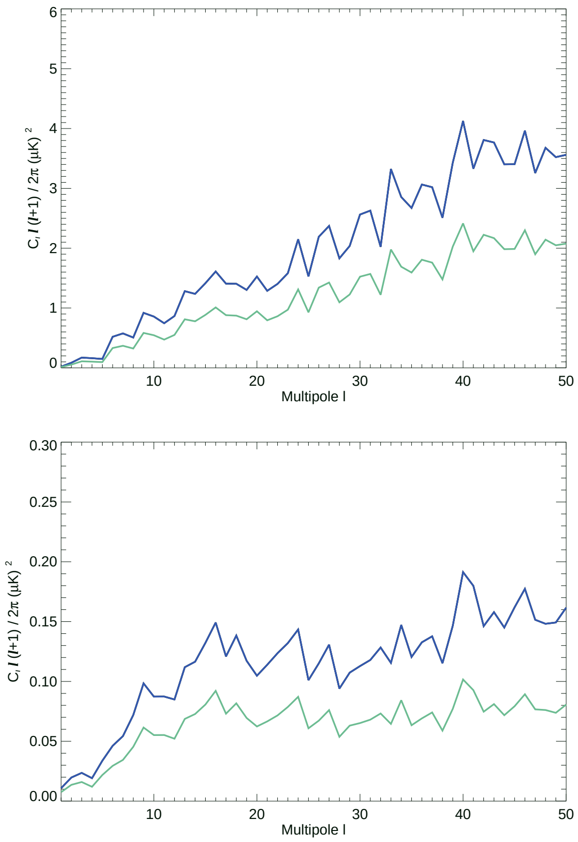

Figure 6. Effects on the power spectra of the inclusion of different physical processes in the constrained simulations of the local universe. Blue and green curves show C_l as extracted from the *gas* and *csf* simulations, respectively. Upper and lower panels refer to the thermal and kinetic SZ effects, respectively. All spectra are taken in the Rayleigh-Jeans region where $\Delta T_{\rm CMB}/T_{\rm CMB} = -2y$.

By comparing the results of our simulation with the estimates obtained by Schaefer et al. (2004), who populated the dark matter only *Hubble volume simulation* (Colberg et al. 2000; Jenkins et al. 2001) with individual, adiabatic cluster simulations, we notice that the SZ effect from the local universe (objects with distance smaller than 110 Mpc from the Milky Way) is the most important contribution up to scales corresponding to $\ell \approx 100$. This is due to the larger angular size of the local supercluster structure. On the contrary, the signal at larger multipoles ($\ell > 200$) seems to be dominated by the more distant sources, which are lying outside of our simulated volume.

In order to evaluate the amount of the signal produced by diffuse gas, we compute $C(\ell)$ from our maps by applying not only the galactic cut, but also masking the regions where the most important local galaxy clusters are. The resulting power spectrum (not shown here) changes drastically for $\ell > 50$ falling off much more rapidly, while remains unchanged for $\ell < 50$. This is an expected result, because the richest clusters are contributing to the power around 2-3 degrees, whereas the total signal from all the rest is dominating the large-scale power.

Having two different constrained realizations of the local universe, the first one with adiabatic physics only, the second one including also cooling, star formation and feedback (the *gas* and *csf* simulations, respectively), it is possible to discuss how the previous results depend on the set of the included physical processes. This is done in Fig.6, where we compare directly the power spectra obtained from the two simulations. We find a higher signal in the adiabatic simulation, both for the thermal and kinetic SZ effects. The amplitude of this difference is very similar in both cases, being approximately a factor of 2. This is in agreement with the results obtained from individual cluster simulations (see, e.g., White et al. 2002). Therefore we do not expect the signal to get stronger when including additional physical processes and we can take the results obtained from the *gas* simulation as a robust upper bound.

4.3 Alignment of lower multipoles

Several anomalies have been detected at low multipoles in the WMAP data. In particular Tegmark et al. (2003) and de Oliveira-Costa et al. (2004) find the CMB quadrupole and octopole to have an unusually high degree of alignment, which is significant at the 2σ level. Moreover they show that the directions of the quadrupole and the octopole are close to the direction of the Virgo cluster which could suggest a possible link to structures in the local universe. By analysing our SZ templates, we find that the directions of the quadrupole and octopole (shown in Fig. 7 for the *gas* simulation) are very different from that extracted from the WMAP data: in our maps the quadrupole and octopole point toward $(b, l) \approx (42.3°, -177.6°)$ and $(b, l) \approx (32.5°, 88.1°)$, respectively, while the preferred axes in the WMAP data are in the directions $(b, l) \approx (58.8°, -102.4°)$ for the quadrupole and $(b, l) \approx (62.0°, -121.6°)$ for the octopole. Moreover the amplitudes of both quadrupole and octopole are far too small to have such an effect.

Finally it has been claimed by different groups that the quadrupole of the CMB is anomalously low [see the discussion in Efstathiou (2004) and references therein] and that this could be caused by structures present in the local universe (Abramo & Sodre 2003). Again, we find that the amplitude of the SZ effect is far too low to have any relevant effect.

4.4 Detectability of the local SZ signal with the Planck satellite

We investigate now whether the local SZ effect can be observed using the upcoming Planck satellite. The very low noise level and the huge frequency range of the Planck experiment could make it capable of seeing this effect at large scales. Note that the CMB itself is the most important contamination when trying to look for the SZ effect at large scales (Hansen et al. 2005). As the CMB has the same temperature at all frequencies, using a map produced by computing the difference between two frequency bands could be a promising way of detecting the SZ effect (this strategy was attempted for the WMAP data in Hansen et al. 2005). This makes the observation of the SZ effect limited only by the instrumental noise. Unfortunately galactic foregrounds also have several frequency dependent components, and these need to be eliminated at a very high degree in order not to confuse detections of the SZ signal. Here we will assume that these have been completely removed outside a conservative galactic cut.

In order to estimate the sensitivity to the local SZ effect for the Planck experiment, we simulated Planck data for the 70, 100, 143 and 217 GHz channels, by using the technical specifications given

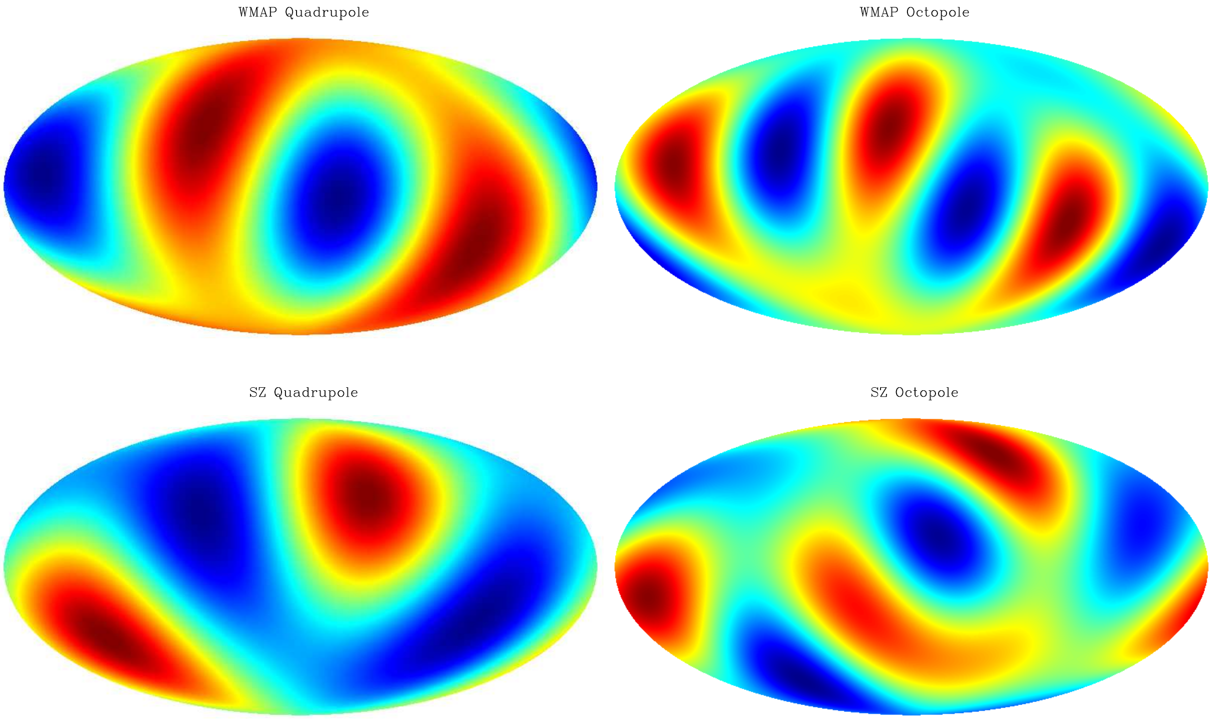

Figure 7. Comparison between the quadrupole (left panels) and octopole (right panels) obtained from the WMAP internal linear combination (ILC) map (upper panels) and from SZ template extracted from the *gas* simulation (lower panels).

at the Planck home page[1]. In more detail, we apply the following procedure.

- For each simulation, we generate a CMB sky and smooth it by using the beams corresponding to the 4 channels of interest.
- We generate white, non-uniform noise for each channel and add it to the maps. The Planck experiment is expected to have highly correlated noise which would affect the noise power spectrum at the largest scales. Since here we are only interested in a rough estimate of the sensitivity of the Planck experiment to the SZ effect, we neglect this effect. Consequently our results could be slightly over-optimistic at the largest scales.
- We add the SZ template to each map by using the frequency dependence of the SZ effect.
- We construct three different maps, corresponding to the difference between the maps at 217 and 100 GHz (called map A), between 143 and 100 GHz (map B) and between 143 and 70 GHz (map C).
- We apply the Kp0 galaxy and point source mask used by the WMAP team (and publicly available at the Lambda website[2]) before calculating the power spectrum of the difference maps.

In Fig. 8 we show the results of a set of 300 different simulations. The solid line corresponds to the power spectrum of the template outside the Kp0 galactic cut. The three shaded areas refer to the 1σ spread from simulations of the three difference maps, map A having the smallest spread, and map C the largest one. We notice that assuming white noise and a perfect foreground subtraction outside the Kp0 cut, we can expect the local SZ effect to be detected by the Planck satellite. Even if real error bars might be larger than our simulations show, one will still be able to compare data with the predicted local SZ effect. Finally note that analyzing difference maps is a useful tool for checking that foregrounds and other systematic effects of the experiment are well understood. For this purpose it will be of high importance to know well the expected local SZ effect as it will give an important contribution to the difference maps.

5 CONCLUSIONS

We used two hydrodynamical cosmological simulations which are designed to represent the observed large-scale structure of the local universe (up to approximately 110 Mpc from the Milky Way) to investigate the imprints of the extended SZ signal caused by local superclusters onto the cosmological full-sky signal. The two simulations, which assume the standard ΛCDM model, started from the same initial conditions, but included the treatment of a different set of physical processes: the first one assumes adiabatic physics only, while the second one follows also cooling, star formation and supernovae feedback.

We find that the largest and most prominent structures observed in the SZ map constructed from our constrained simulations are caused by local superclusters like Pisces-Perseus or the Centaurus supercluster region. Even Virgo, a relatively poor but nearby cluster, belongs to the most prominent and extended features of the map. Comparing the power spectra of the thermal SZ signal with the one derived from the *Hubble volume simulation* (Schaefer et al. 2004), we find that for $\ell < 100$ these structures lead to an am-

[1] http://www.rssd.esa.int/index.php?project=PLANCK
[2] http://lambda.gsfc.nasa.gov/

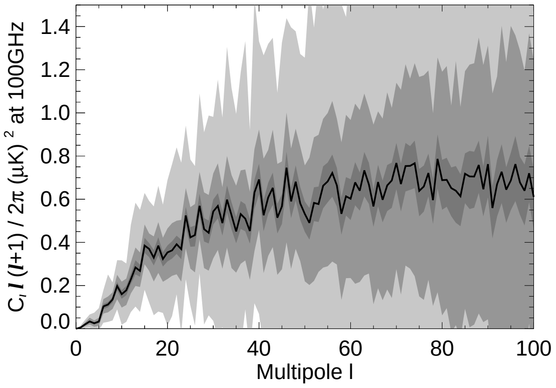

Figure 8. The estimated power spectra of three difference maps from Planck simulations. The solid line shows the power spectrum of the local SZ template. The shaded bands correspond to the 1σ spread of the estimated power spectra in 300 simulations for the following difference maps: A = 217-100 GHz, B = 143-100 GHz and C = 143-70 GHz. Map A has the lowest spread and map C has the largest one. The Kp0 galactic cut has been used in these simulations. Note that all spectra are normalized to the expected SZ effect at 100 GHz.

plitude which is at least twice as high (one order of magnitude for $\ell < 20$). When comparing the derived power spectra for the kinetic SZ this factor is even higher.

However, the overall amplitude of the effect is far too small (3-4 orders of magnitude) to have any significant influence on the lowest multipoles of the CMB. There have been some claims that the anomalously low CMB quadrupole and octopole observed by the WMAP satellite could be explained by the imprints of local superclusters. We have shown that the amplitude of the SZ low multipoles must be considerably much higher in order to produce such an effect as well as to have an influence on the observed quadrupole and octopole. Moreover, the directions on the sky of the quadrupole and octopole inferred from our simulations do not coincide with the observed direction in the WMAP maps.

Both for our *gas* simulation as well as for the *Hubble volume simulation*, radiative cooling processes and feedback by star formation have been neglected, which could change the absolute amplitude of the inferred SZ signal of galaxy clusters. However, using a simulation which includes all these effects (the *csf* simulation), we even find a slight decrease of the SZ signal, similar to the findings obtained by using isolated cluster simulations. This will make it even more unlikely to explain the abnormal lower multipoles observed in the WMAP data with the SZ signal of the local universe.

Nevertheless, we find that when taking advantage of the huge frequency range and low noise level of the Planck satellite, an estimate of the SZ power spectrum at large scales could be obtained. We have shown this by producing a set of simulated CMB maps with experimental noise at several frequencies. Analyzing the power spectrum of maps obtained by taking the difference of CMB maps at different frequencies, we show that the power spectrum of the SZ effect is limited only by experimental noise and foreground contamination. We have found that the predicted noise level of the Planck satellite is low enough to allow for the detection of the local SZ power spectrum at low multipoles provided that the galaxy can be removed with sufficient accuracy. It is out of the scope of this work to obtain an accurate estimate of the predicted detection level by the Planck satellite, for which correlated noise as well as an accurate study of foreground removal procedures is required.

ACKNOWLEDGEMENTS

We would like to thank Bjoern Schäfer for providing the SZ maps derived from the *Hubble volume simulation* and the MPAC team at MPA for the access to analysis software. We are also grateful to A. Banday for a critical reading of the manuscript and useful discussions. The hydrodynamical simulations presented in this work have been performed using computer facilities at the Rechenzentrum der Max-Planck-Gesellschaft, Garching (the *gas* simulation), and at the University of Tokyo supported by the Special Coordination Fund for Promoting Science and Technology, Ministry of Education, Culture, Sport, Science and Technology (the *csf* simulation). KD acknowledges partial support by a Marie Curie Fellowship of the European Community program "Human Potential" under contract number MCFI-2001-01227. FKH acknowledges financial support from the Norwegian Research Council. We acknowledge use of the HEALPIx (Górski et al. 1998) software and analysis package for deriving the results in this paper.

REFERENCES

Abramo R., Sodre J., 2003, preprint, astro-ph/0312124
Afshordi N., Loh Y., Strauss M. A., 2004, Phys. Rev. D, 69, 083524
Bartelmann M., 2001, A&A, 370, 754
Battistelli E. S., De Petris M., Lamagna L., Luzzi G., et al., 2003, ApJ, 598, L75
Bennett C., Bay M., Halpern M., Hinshaw G., et al., 2003, ApJ, 583, 1
Colberg J. M., White S. D. M., Yoshida N., MacFarland T. J., et al., 2000, MNRAS, 319, 209
Cooray A., Baumann D., Sigurdson K., 2004, preprint, astro-ph/0410006
da Silva A. C., Kay S. T., Liddle A. R., Thomas P. A., 2004, MNRAS, 348, 1401
de Oliveira-Costa A., Tegmark M., Zaldarriaga M., Hamilton A., 2004, Phys. Rev. D, 69, 063516
Diego J. M., Silk J., Sliwa W., 2003, New Astronomy Review, 47, 855
Dolag K., Grasso D., Springel V., Tkachev I., 2005, JCAP, 1, 9
Efstathiou G., 2004, MNRAS, 348, 885
Efstathiou G., 2004, MNRAS, 348, 885
Fosalba P., Gaztañaga E., 2004, MNRAS, 350, L37
Gaztañaga E., Wagg J., Multamäki T., Montaña A., Hughes D. H., 2003, MNRAS, 346, 47
Górski K. M., Hivon E., Wandelt B. D., 1998, 'Analysis Issues for Large CMB Data Sets', 1998, eds A. J. Banday,R. K. Sheth and L. Da Costa, ESO, Printpartners Ipskamp, NL, pp.37-42 (astro-ph/9812350); Healpix HOMEPAGE: http://www.eso.org/science/healpix/
Hansen F. K., Branchini E., Mazzotta P., Cabella P., Dolag K., 2005, MNRAS, submitted, astro-ph/0502227
Hernández-Monteagudo C., Rubiño-Martín J. A., 2004, MNRAS, 347, 403
Hernandez-Monteagudo C., Genova-Santos R., Atrio-Barandela F., 2004, preprint, astro-ph/0406428

Hirata C. M., Padmanabhan N., Seljak U., Schlegel D., Brinkmann J., 2004, Phys. Rev. D, 70, 103501
Hoffman Y., Ribak E., 1991, ApJ, 380, L5
Huffenberger K. M., Seljak U., Makarov A., 2004, Phys. Rev. D, 70, 063002
Ikebe Y., Reiprich T. H., Böhringer H., Tanaka Y., Kitayama T., 2002, A&A, 383, 773
Jenkins A., Frenk C. S., White S. D. M., Colberg J. M., Cole S., Evrard A. E., Couchman H. M. P., Yoshida N., 2001, MNRAS, 321, 372
Kolatt T., Dekel A., Ganon G., Willick J. A., 1996, ApJ, 458, 419
Mathis H., Lemson G., Springel V., Kauffmann G., White S. D. M., Eldar A., Dekel A., 2002, MNRAS, 333, 739
Mazzotta P., Rasia E., Moscardini L., Tormen G., 2004, MNRAS, 354, 10
Mohr J. J., Mathiesen B., Evrard A. E., 1999, ApJ, 517, 627
Monaghan J. J., Lattanzio J. C., 1985, A&A, 149, 135
Motl P. M., Hallman E. J., Burns J. O., Norman M. L., 2005, ApJ, 623, L63
Myers A. D., Shanks T., Outram P. J., Frith W. J., Wolfendale A. W., 2004, MNRAS, 347, L67
Rasia E., Mazzotta P., Borgani S., Moscardini L., Dolag K., Tormen G., Diaferio A., Murante G., 2005, ApJ, 618, L1
Sanderson A. J. R., Ponman T. J., Finoguenov A., Lloyd-Davies E. J., Markevitch M., 2003, MNRAS, 340, 989
Schaefer B. M., Pfrommer C., Bartelmann M., Springel V., Hernquist L., 2004, preprint, astro-ph/0407089
Spergel D. N., Verde L., Peiris H. V., Komatsu E., et al., 2003, ApJS, 148, 175
Springel V., 2005, preprint, astro-ph/0505010
Springel V., Hernquist L., 2002, MNRAS, 333, 649
Springel V., Hernquist L., 2003, MNRAS, 339, 289
Springel V., Yoshida N., White S., 2001, New Astronomy, 6, 79
Sunyaev R. A., Zeldovich Y. B., 1972, Comments on Astrophysics and Space Physics, 4, 173
Tegmark M., de Oliveira-Costa A., Hamilton A., 2003, Phys. Rev. D, 68, 123523
Tornatore L., Borgani S., Matteucci F., Recchi S., Tozzi P., 2004, MNRAS, 349, L19
Tornatore L., Borgani S., Springel V., Matteucci F., Menci N., Murante G., 2003, MNRAS, 342, 1025
Vikhlinin A., 2005, preprint, astro-ph/0504098
White M., Hernquist L., Springel V., 2002, ApJ, 579, 16